metals

MDPI

Review

Factors Affecting the Surface Roughness of the As-Built Additively Manufactured Metal Parts: A Review

Simone Paggetti [1,*], Enrico Bedogni [1,2] and Paolo Veronesi [1]

[1] Department of Engineering 'Enzo Ferrari', Universita degli Studi di Modena e Reggio Emilia, 41125 Modena, MO, Italy; enrico.bedogni@kosme.it (E.B.); paolov@unimore.it (P.V.)
[2] Kosme s.r.l. Unipersonale, Via dell'Artigianato, 5, 46048 Roverbella, MN, Italy
* Correspondence: simone.paggetti@unimore.it

Abstract

Nowadays, additive manufacturing technologies continue to increase in number, and with them, the various challenges they bring for the optimal design of components. However, many relevant applications require that a certain surface finishing level is reached; in particular, surface roughness should stay below a certain threshold. The aim of this work is to provide, for each of the most used metal additive manufacturing technologies, a short review of parameters affecting as-built surface roughness, indicating possible correlations with process parameters. The identified correlations, summarized visually as tables, could serve as starting guidelines for the design and production of parts with controlled surface roughness or having a surface roughness suitable for the application of possible surface finishing post-processes.

Keywords: additive manufacturing; surface roughness; power bed fusion; direct energy deposition; binder jetting; material extrusion; layer laminate manufacturing; surface finishing

Academic Editors: Petru Berce and Răzvan Păcurar

Received: 19 August 2025
Revised: 18 September 2025
Accepted: 22 September 2025
Published: 24 September 2025

Citation: Paggetti, S.; Bedogni, E.; Veronesi, P. Factors Affecting the Surface Roughness of the As-Built Additively Manufactured Metal Parts: A Review. *Metals* **2025**, *15*, 1069. https://doi.org/10.3390/met15101069

1. Introduction

Additive Manufacturing (AM) is a production process that creates three-dimensional objects by adding material layer by layer, unlike subtractive manufacturing, where material is removed from a solid block to achieve the desired shape. It is commonly used for prototyping, given its flexibility in creating a wide variety of geometries, but also for standard parts production. Parts made using AM are particularly recognizable because the production method is clearly reflected on the 'as-built' surface, which usually shows the construction layers used. The roughness of surfaces produced by metal AM is influenced by many parameters, among which [1]:

- Technology.
- Raw materials: type, shape (wire, sheets, or powders), and dimensions or particle size.
- Process-related parameters such as energy density, layer thickness, and building speed.
- Parts-related parameters, such as the presence of inclined surfaces, supports, etc.

The ones listed above are the ones with the greater impact, but many more have a smaller role, such as building strategies within each layer, orientation in the building plate, inert gas flow, etc.

Surface roughness plays a critical role in determining the functional performance, reliability, and quality of components across a wide range of industrial sectors. In mechanical engineering, rough surfaces can lead to increased friction, wear, and premature fatigue

failure of moving parts. This is particularly problematic in precision assemblies, where tight tolerances and smooth interactions are essential for optimal operation [2–4].

In the aerospace industry, surface roughness directly influences aerodynamic performance. Components such as turbine blades, airframes, and nozzles require extremely smooth surfaces to minimize drag and improve fuel efficiency. Even minor deviations in surface texture can lead to turbulent airflow, increased energy consumption, and reduced operational lifespan [5–7].

The food industry also faces challenges related to surface roughness, especially in equipment used for processing, packaging, and handling. Rough surfaces can harbor contaminants and microorganisms, making cleaning and sterilization more difficult. This not only compromises hygiene standards but also increases the risk of product contamination and regulatory non-compliance. A direct example is the requirement for a specific surface roughness value when food products come into direct contact with metallic components [8–10].

In the medical field, implants and surgical tools must exhibit controlled surface roughness to ensure biocompatibility and proper integration with biological tissues. Excessive roughness can lead to inflammation, poor healing, or rejection, while insufficient roughness may hinder cell adhesion and osseointegration [11–13].

Surface roughness also affects coating adhesion, corrosion resistance, and fatigue strength in automotive and marine applications. For instance, rough substrates may lead to uneven coating thickness, resulting in weak spots and accelerated degradation under environmental stress [14–16].

Moreover, in additive manufacturing, surface roughness is a key parameter influencing post-processing requirements, dimensional accuracy, and mechanical properties. Various technologies exhibit different degrees of surface roughness depending on process parameters, material properties, layer resolution, etc.

Despite its importance, surface roughness is often under-characterized in industrial studies. More comprehensive investigations are needed to understand its behavior under different processing conditions and its long-term impact on component performance.

In conclusion, surface roughness is a multifaceted issue that affects product quality, safety, and efficiency across diverse industries. Addressing it through improved design, material selection, and process control is essential for advancing manufacturing technologies and meeting increasingly stringent performance standards.

Concerning technologies, the most widely used for metal parts are Powder Bed Fusion (PBF), Direct Energy Deposition (DED), Binder Jetting (BJ) and Material Extrusion (ME).

PBF technologies are a group of additive manufacturing techniques that produce 3D parts from powder materials. The laser source is fixed, and the beam is directed across the printing bed using a system of lenses [17]. Among the PBF technologies, the most relevant are:

- Selective Laser Melting (SLM). This technology uses one or more lasers to melt layers of metal powder. The laser focuses on a single spot, melting the powder with an average layer thickness between 30 and 60 μm or larger [18]. The laser spot is circular and can vary in diameter from 20 to 200 μm.
- Area Wise Laser Powder Bed Fusion (AWLPBF)/Diode-based Additive Manufacturing (DiAM). Also called area printing LPBF, this technology uses a wide pulsed beam composed of multiple lasers to create an image of approximately 1 cm^2 that melts the powder. The layer thickness ranges between 50 and 100 μm [19].
- Electron Beam Melting (EBM) uses an electron beam as a heat source instead of a laser. The beam focuses on a single point, similarly to SLM. Unlike the typical argon-shielded

chamber, EBM operates in a vacuum. Common layer thickness ranges between 50 and 100 µm [20].

Selective Laser Sintering (SLS) technologies, while architecturally similar to SLM, and thus typically listed among the PBF methods, SLS does not fully melt the metal powders. There are many ways to realize metal components by sintering. In Solid State Sintering, the part is formed at the sintering temperature of the printing metal, and the raw material is just made of the metal powder in which the components are printed. In Chemically Induced Binding, chemical reactions occurring between the material powders or between the powders and the atmosphere of the printing chamber are used to impart form to the powders. The products of these reactions act as binders for the primary powders. In Liquid Phase Sintering/Partial Melting, there are three further subclasses according to the type of powder grains used: separate grains, composite grains, and coated. These three categories explain how the binder and powder material are mixed or prepared before printing. In this case, the binder can be polymeric or metallic [21].

Direct Energy Deposition (DED) technologies are a group of additive manufacturing techniques that build 3D objects using either powders or wire as raw materials, usually assisted by a laser as a heat source. Unlike PBF, in DED the material is deposited and melted simultaneously, and the heat source is mobile, moving across the printing area. The layer thickness in DED processes is typically in the millimeter or sub-millimeter range, which is significantly higher than in PBF. These technologies are particularly efficient for adding material only where needed, making them well-suited for repair applications or for building large, near-net-shape components [17,22]. Among the DED techniques, the most widely used are:

- Laser Metal Deposition (LMD)/Laser-engineered net shaping (LENS)/Powder Laser Energy Deposition (PLED): in this process, the raw material—typically metal powder—is melted by a laser and simultaneously deposited onto a substrate to build the part layer by layer [23].
- Wire Laser Energy Deposition (WLED)/Wire Laser Additive Manufacturing (WLAM): This technique operates similarly to LMD but uses metal wire instead of powder as the feedstock. The wire is melted by a laser during deposition.
- Wire Electron Beam Energy Deposition (WEBED)/Wire Electron Beam Additive Manufacturing (WEBAM)/Electron Beam Freeform Fabrication (EBF^3)/Electron Beam Wire-Feed Additive Manufacturing (EBWFAM): A wire feedstock is melted using an electron beam rather than a laser. Due to the need for a vacuum environment to operate the electron beam, powder-based deposition (as in LMD) is not feasible [24].
- Wire Arc Additive Manufacturing (WAAM): This process employs a Gas Metal Arc Welding (GMAW) torch mounted on a robotic arm. Similar to conventional welding, the electric arc is shielded using inert gas [22].
- Submerged Arc Additive Manufacturing (SAAM): while the hardware setup is similar to WAAM, this method replaces the inert gas shielding with a layer of sand that submerges the melt pool, thereby protecting it from oxidation [25].
- Rapid Plasma Deposition (RPD)/Wire Plasma Arc Energy Deposition (WPAED)/Plasma Metal Deposition (PMD): this variant uses a Gas Tungsten Arc Welding (GTAW) torch instead of GMAW, while maintaining the same general configuration as WAAM [26].
- Metal Powder Application (MPA), also known as Cold Spray Additive Manufacturing (CSAM): A variant of DED, using kinetic energy instead of a heat source alone. It employs a high-velocity gas stream to accelerate metal powder particles toward a substrate, where they accumulate to form the desired component. Upon impact, the particles undergo severe plastic deformation, converting kinetic energy into localized thermal energy, which facilitates bonding without melting. Originally developed for

coating applications, this solid-state process has since been adapted for additive manufacturing, particularly for materials that are difficult to process using conventional fusion-based techniques [27,28].

Binder technologies utilize metal powders combined with a binder, which imparts sufficient mechanical strength to the green parts prior to sintering. On average, the layer thickness used in these processes ranges between 50 and 100 µm. In most cases, a debinding step is required either before or during the sintering phase to remove the binder and ensure proper densification of the final component, or impregnation with a lower melting point metal is performed alternatively to sintering. Among these technologies, the most relevant are:

- Metal Binder Jetting (MBJ): This process spreads a layer of metal powder and selectively deposits binder only where the part is to be formed. The binder is then activated using a heat source, typically a lamp. MBJ does not require support structures [29].
- Mold Slurry Deposition (MSD)/MoldJet (MJ)/Layerwise Slurry Deposition (LSD): In this method, metal powder and binder are pre-mixed into a slurry. A wax mold is first created additively using a drop-on-demand technique and then filled with slurry. The wax mold provides integrated support during printing [30].
- Lithography-based Metal Manufacturing (LMM)/Area Wise Vat Polymerization (AWVP)/Digital Light Processing (DLP)/Vat Photo Polymerization (VPP): Even if not commonly listed among the BJ technologies, it combines metal powders and binders, and it is here included for this reason. This technology uses a photopolymerization process similar to Stereolithography (SLA). Metal powder is suspended in a photopolymer binder, which is selectively cured by light exposure. LMM is the only technology among these that requires support structures [31].
- Material Jetting (MJ)/Metal Material Jetting (MMJ). This technique is very similar to Metal Binder Jetting (MBJ). Instead of using a recoater that deposits only metallic powder, which is subsequently impregnated with a binder, MMJ employs a slurry in which the binder and metallic powder are pre-mixed. This mixture is deposited through a series of nozzles, like MBJ. Additionally, a second set of nozzles is used to deposit support material. The powders used in this technology are typically very fine, often in the nanometric range, as they must be able to pass through the narrow nozzles required by jetting systems [32,33].

Material Extrusion (ME) technologies are polymer additive manufacturing processes, such as extrusion and jetting-based methods, which have been adapted for metal printing. These technologies share the need for post-processing steps such as debinding and sintering to remove the binder and densify the final part or, alternatively, impregnation. Among them:

- Fused Deposition Modeling (FDM)/Filament Material Extrusion (FME), also known as Fused Filament Fabrication (FFF): It is one of the most widely used 3D printing technologies. It operates by extruding a thermoplastic filament through a heated nozzle, depositing material layer by layer onto a build platform. When applied to metal printing, the filament is loaded with metal powder [34].
- Pellet Material Extrusion (PME): follows the same principle as FDM, but the feedstock is in the form of pellets rather than filament, offering potential advantages in terms of material cost and feed flexibility.
- Dispersion Material Extrusion (DME): Follows the same architecture of the previous two technologies; instead of using a polymer as a binder during extrusion, a liquid binder is employed, resulting in a metallic powder dispersed in the form of a slurry.

This slurry is then deposited onto the build platform via an extruder, similarly to a conventional FME process [35].

Layer Laminate Manufacturing (LLM), also referred to as Sheet Lamination (SL), is an additive manufacturing process used to fabricate three-dimensional objects by stacking and bonding successive layers of material. The process begins with sheets of material-typically paper, plastic, or metal foil-which are layered and bonded using techniques such as adhesive application, ultrasonic welding, heat, or pressure. Each sheet is precisely cut to the desired geometry either before or after the bonding step. This method is considered a hybrid additive-subtractive technique, as it involves both the addition of material through layering and the removal of excess material during the cutting phase [17], and it will be excluded from this review.

Friction Energy Deposition (FED), Friction Stir Additive Manufacturing (FSAM), Friction Stir Powder Additive Manufacturing (FSPAM), or Additive Friction Stir Deposition (AFSD): This technology utilizes the energy generated by friction resulting from the rotation of the deposition head against the build platform initially, and subsequently against the underlying layers [36]. It operates either with a feedstock in the form of rods or powder, or in combination with LLM as a method for welding metallic sheets [37,38].

Liquid Metal Printing (LMP), Direct Metal Writing (DMW), Drop-On-Demand Liquid Metal Jetting (DOD-LMJ) or Molten Metal Jetting (MMJ): This technology resembles Drop-on-Demand (DoD) printing where the feedstock was replaced by molten metal [39]. This makes it challenging to work with metals that have high melting points. As a result, one of the most commonly used materials is aluminum and its alloys [40,41].

Localized Electrodeposition in Liquid (LEL), Localized Electrochemical Deposition (LECD): It utilizes a conductive substrate immersed in a liquid electrolyte. The extrusion head injects a metal solution that is electrochemically deposited onto the substrate, which acts as the cathode, while the anode is positioned around the perimeter of the build area, separated by an insulating layer. This submicrometric technique is patented by Exaddon [42]. Although its industrial application is currently limited due to the small build volume and low production speed, this technology has been included in the overview of metal additive manufacturing methods for completeness. Nevertheless, it finds application in the medical field [43,44].

Figure 1 presents all the technologies mentioned above.

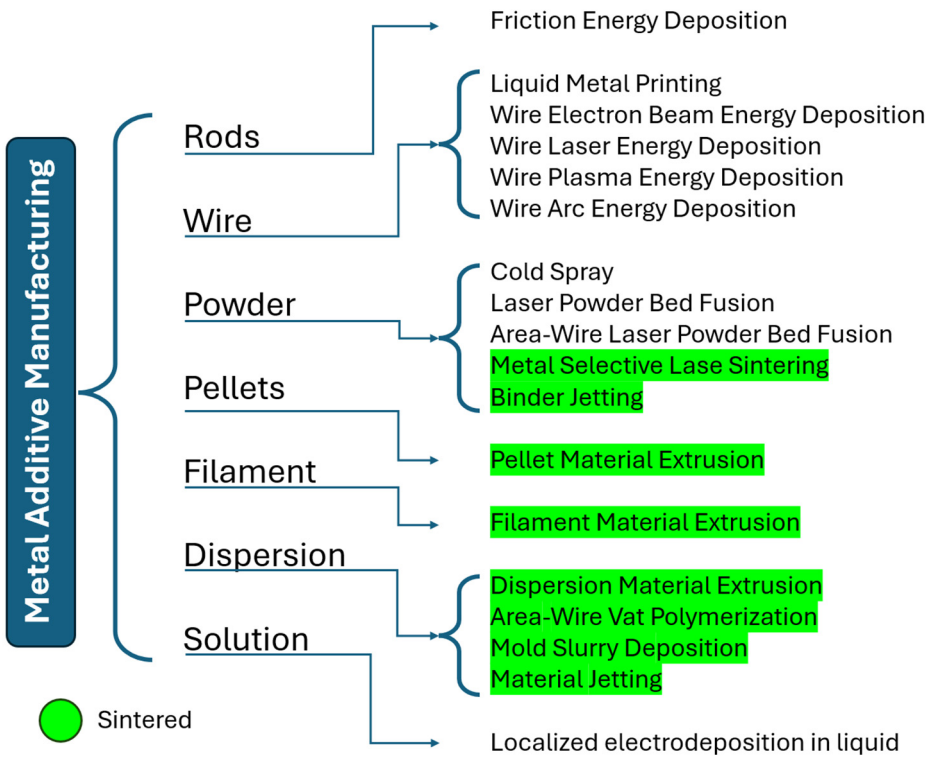

Figure 1. Overview map of AM technologies.

2. As-Built Surface Roughness

2.1. Selective Laser Melting

Starting with SLM technologies, the effect of processing parameters on surface roughness has been widely investigated. Hatching spacing, scan speed, and laser power effects were recently studied by Mansoura et al. by analyzing the effect of two parameters at a time, while keeping the layer thickness constant at 40 µm [18]. Measurements were taken on the 0° up-skin surface. The reported values by Mansoura et al. for 316L stainless steel powder show an average roughness (Ra) ranging from 4.30 to 6.47 µm. The analysis of the three contour plots reported in that study highlights the influence of process parameters on surface roughness, showing that increasing both hatching spacing and scan speed is responsible for an increase in the as-built surface roughness. The same study explores the relationship between laser power and hatch spacing, and it demonstrates that roughness decreases with increasing laser power but increases with increasing hatch spacing. In the case of the combined effects of laser power and scan speed, as expected, roughness increases when laser power increases and scan speed increases.

The combination of the three plots provides useful information for the combined optimization of these parameters, providing a more detailed insight into the process with respect to the energy density parameter alone. Overall, the interaction plots of this study serve as a fundamental tool for identifying optimal operating conditions aimed at minimizing surface roughness, thereby contributing to the improvement of additive manufacturing or laser processing surface quality [45]. However, these studies contrast with the findings of Correa-Gómez et al. and Yildiz et al., which report opposite effects in response to changes in energy density, despite similar trends in scan speed, hatch spacing, and laser power. In this case, a reduction in surface roughness was observed with decreasing laser power and increasing scan speed [46,47].

This shift in the effect of process variables at different energy densities can be attributed to changes in melt pool behavior, as demonstrated in Jiang et al. studies. It is shown that,

at both high and low energy densities, fusion defects can occur—ranging from unmelted powder to open surface porosity—which contribute to the final surface roughness of the as-built component [48].

This encourages the search for an optimal intermediate energy density that can yield the best possible as-built surface roughness.

As previously mentioned, another variable that influences surface roughness is the geometry of the component and, specifically, the inclination of the surface relative to the printing plate.

This correlation was studied by Wang et al. [19], who demonstrated that surface roughness can increase by up to a factor of 10 when comparing the best and worst surface orientations. For up-skin surfaces, the average roughness (Ra) measured for processing 316L stainless steel powders ranges from 5.03 µm to 24.2 µm, while the Rz values range from 12.7 µm to 55.90 µm. Similar trends were observed for down-skin surfaces, where Ra values range from 6.25 µm to 65.10 µm, and Rz values range from 15.80 µm to 230.00 µm [49].

The last variable considered is the metal powder particle size, which also plays a significant role in surface roughness, not only because it practically sets a lower limit to PBF layer thickness.

For SLM, the commonly used particle size distribution has a D10 of 15 µm and a D90 of 45 µm, often referred to as 15–45. In their study, Sinico et al. [20] analyzed three different Maraging 300 powder size distributions: 15–45 µm, 10–30 µm, and 5–15 µm. The finest distribution, 5–15 µm, was excluded from further analysis due to its poor flowability, which negatively affects the powder spreading process during printing [50]. Considering all tested combinations of energy density and laser power, specimens fabricated with smaller particles consistently exhibited higher surface quality, with a reduction in Ra ranging from approximately 20% to over 50% with respect to the coarser particles.

The following table (Table 1) summarizes the main findings of the aforementioned studies:

Table 1. Effect of SLM processing parameters of steel powders on the as-built surface.

Variables	Action	Effect	Physical Mechanisms Involved
Hatching spacing	Increase	Increase roughness	Melt pool behavior
Scan speed (Low J/mm^3)	Increase	Increase roughness	Melt pool behavior
Laser power (Low J/mm^3)	Increase	Decrease roughness	Melt pool behavior
Scan speed (High J/mm^3)	Increase	Decrease roughness	Melt pool behavior
Laser power (High J/mm^3)	Increase	Increase roughness	Melt pool behavior
Surface angles	Approach 0° and 90°	Decrease roughness	Gravity on melt pool
Particle size	Decrease	Decrease roughness	Powder packing
Particle size	Too small	Poor flowability	Powder rheology

2.2. Area Wise Laser Powder Bed Fusion

This technology was developed and patented by Seurat [19,51]. Currently, there are no published studies specifically analyzing surface roughness for this process.

However, since it employs a layer-by-layer approach with a layer thickness range similar to other LPBF techniques, it is plausible that the surface roughness for up-skin and down-skin surfaces at various angles is of the same order of magnitude, except for the 0° up-skin and 90° vertical surfaces. These two orientations are significantly influenced by the laser scanning pattern and the melt pool dynamics, which differ substantially from those in conventional L-PBF systems.

Few papers have been published on this technology, and even fewer have focused on surface roughness. However, the works by Fotovvati et al. and Matthews et al. report

roughness values for 0° up-skin surfaces, varying with energy density, ranging from 1.7 to 10 µm [52] and the Spearman correlation matrix for the technology's parameter [51].

2.3. Electron Beam Melting

Compared to SLM technologies, the greater layer thickness used in EBM has a direct impact on surface roughness. While EBM is typically better suited for mass production thanks to its higher build rate, it also tends to result in increased roughness [53].

Due to the ferromagnetic nature of steels, they are rarely used in Electron Beam Melting (EBM). As a result, only a limited number of studies have been conducted on this material. For this reason, Ti-6Al-4V alloy was selected for investigation in the context of EBM.

The influence of various process parameters on surface roughness in EBM of Ti-6Al-4V was investigated using powders with a particle size distribution of 50–100 µm. According to Safdar et al. and Wang et al. [54,55], the average surface roughness (Ra) ranged from 2 to 24 µm. No Rz values were reported, and the study includes only vertical surfaces. Nevertheless, the study illustrates the variation of surface roughness (Ra) as a function of different process conditions. The influence of material thickness was investigated by comparing two configurations: 5.5 mm and 7.5 mm thick samples. Results demonstrate that lowering the thickness reduces roughness. The same study addresses the effect of electrical current, comparing the use of 6 mA and of 4 mA on samples having the same thickness. Results show that roughness is decreased when reducing the current. Moreover, results show that a faster scan speed improves surface quality. Finally, the influence of focus offset is investigated, resulting in a surface roughness reduction when using a larger offset focus. Collectively, these findings provide a comprehensive overview of how variations in thickness, current, scan speed, and focus offset affect surface roughness. The primary factor contributing to the increase in surface roughness is the thermal load on the material, which leads to the sintering of loose powder particles on the surface [55].

The study conducted by Galati et al. [53] focused on the influence of part geometry on surface roughness for Ti-6Al-4V. In their experiments, the average particle size was 75 µm, and the layer thickness was fixed at 50 µm. The analyses were conducted on surfaces with varying inclinations, ranging from the horizontal up-skin surface up to an angle of 60° and from 80° to 50° for down-skin surfaces.

For upward-facing surfaces, the average roughness (Ra) was 14.922 µm, with a standard deviation of 0.657 µm. In contrast, downward-facing surfaces exhibited a higher average Ra of 19.133 µm, with a standard deviation of 0.306 µm. The main factor responsible for the increase in surface roughness is the staircase effect [53].

The following table (Table 2) summarizes the main findings of the aforementioned studies:

Table 2. Effect of EBM processing parameters on the as-built surface of Ti6Al4V samples.

Variables	Action	Effect	Physical Mechanisms Involved
Sample thickness	Increase	Increase roughness	Component core sintering surroundings
Current	Increase	Increase roughness	Melt pool sintering surroundings
Scan speed	Increase	Decrease roughness	Melt pool sintering surroundings

Table 2. *Cont.*

Variables	Action	Effect	Physical Mechanisms Involved
Offset focus	Increase	Decrease roughness	Melt pool sintering surroundings
Surface angles (Up-skin)	From 0° to 90°	Increase roughness	Staircase effect
Surface angles (Down-skin)	From 90° to 180°	Roughness: Maximum at the extremes and central minimum	Staircase effect

2.4. Selective Laser Sintering

Due to the specific sub-category of binding methods that do not fully melt the metal powder—or only melt the binder component—Selective Laser Sintering (SLS) is considered separately from other Laser Powder Bed Fusion (L-PBF) techniques in this study.

Among the various bonding systems, this work focuses on those most commonly used for the manufacturing of metal components, starting with metal powders, either coated with a binder or not [21].

Like L-PBF, the main parameters influencing surface roughness in SLS are energy density and its related variables, such as laser power, layer thickness, scan speed, hatch spacing, and spot size. Additional factors include part bed temperature and scan strategy.

Wang et al. investigated an iron-based powder blend containing 29% Nickel, 8.3% Copper, and 1.35% Phosphorus. Their study reported surface roughness values for 0° up-skin surfaces and those perpendicular to the build direction. The average roughness was 18.2 μm for the top view and 12.6 μm for the side view. These values were primarily attributed to thermal stresses that caused surface cracking. Pores formed during sintering were correlated with the build direction, with areas ranging from approximately 120 ± 280 μm^2 on the top surface and 57 ± 114 μm^2 on the side surface. Pore formation was most prevalent between layers [56].

A comprehensive study by Sachdeva et al. [57] focused on the roughness of 0° up-skin surfaces in SLS, analyzing additional parameters such as bed temperature, hatch length, and scan count. Their reference energy density was 28 J/mm^2, significantly higher than that used in Song and Koenig's work [58]. Sachdeva's findings illustrate the trends of Ra and Rz roughness values as functions of laser power, hatch spacing, bed temperature, and hatch length. The variation of the aforementioned process parameters affected both Ra and Rz similarly. The reference values were 28 W laser power (ranging from 24 to 32 W), 0.2 mm hatch spacing (ranging from 0.1 to 0.3 mm), 175 °C bed temperature (ranging from 172 to 178 °C), and 100 mm hatch length (ranging from 40 to 120 mm). Ra and Rz both showed a maximum at the reference laser power and a minimum with lower scan speed and bed temperature. Hatch length exhibited a progressive reduction in roughness with increasing values. The only notable difference was that the Rz maximum was slightly shifted to a higher laser power compared to Ra [57].

The roughness values reported in both studies ranged from 5.46 to 18.2 μm for Ra and from 30.87 to approximately 160 μm for Rz [57,58].

From the work of Attarzadeh et al., it is possible to derive the trends in surface roughness for surfaces parallel to the build plate, under even higher energy densities—effectively continuing the investigation initiated by Song and Koenig. Across this entire energy range, a reduction in surface roughness is observed, attributed to the removal of defects [59].

Zhu et al. conducted extensive research on the sintering of coated metal powders. Their findings indicate that varying binder contents have a direct impact on the maximum

sintering temperature, along with the particle size distribution of the powders used. Powders with an average size of 14.2 µm do not exhibit lower thermal stability compared to those of 22 µm, yet they produce components with higher density at lower temperatures and offer a superior surface finish, 1.72 µm [60]. This technique does not directly modify the metal powders through laser interaction; therefore, the printing parameters are of secondary importance.

The following table (Table 3) summarizes the main trends that emerged from the literature search:

Table 3. Effect of SLS processing parameters on the as-built surface.

Variables	Action	Effect	Physical Mechanisms Involved
Laser power	Increase	Roughness: Maximum at reference point parameters (28 J/mm^2)	Low and high energy create defects through unsintered or stick powder
Hatch spacing	Increase	Roughness: Minimum at reference point parameters (28 J/mm^2)	Low and high energy create defects through unsintered or stick powder
Hatch length	Increase	Decrease roughness	Melt pool behavior
Bed temperature	Increase	Roughness: Minimum at reference point parameters (28 J/mm^2)	Low and high energy create defects through unsintered or stick powder

2.5. Laser Metal Deposition

In blown 316L stainless steel and Inconel 718 powder DED components, surface roughness (Ra) values have been reported to range between 17 and 110 µm [61].

The main DED process parameters influencing surface roughness, as analyzed by Jardon et al. [62], include:

- $\dot{m}_p$: powder mass flow
- $\dot{V}_{CG}$: carrying gas flow
- $\dot{V}_{SG}$: shielding gas flow
- Particle size distribution
- Presence of residual unmelted powder

These factors collectively affect the consistency of material deposition and the quality of the melt pool, which in turn influences the final surface finish.

An important factor influencing surface roughness in DED is the ratio between the carrying gas flow rate and the shielding gas flow rate. When $\dot{V}_{CG}/\dot{V}_{SG}$ ratio is high, the melt pool tends to be more uniform, with a circular front boundary, indicating stable powder delivery and consistent melting. Conversely, when the ratio is low, powder convergence decreases, resulting in less powder reaching the melt pool, which can lead to irregular deposition and increased surface roughness [62].

Powder particles can also adhere to the surface of the melt pool, contributing to an increase in overall surface roughness. This phenomenon is more pronounced with larger particles, which are more likely to remain partially melted or unmelted on the surface. In contrast, smaller particles tend to have a lower impact, as they are more easily absorbed into the melt pool and less likely to stick to the surface [62–64].

As studied by Jardon et al., increasing the powder mass flow rate ($\dot{m}_p$) correlates with an increase in surface roughness. At low mass flow rates, particles behave more like individual entities rather than a continuous stream, making them more likely to remain attached to the melt pool surface. At higher mass flow rates, although the force required to overcome the melt pool's surface tension is lower, the greater number of particles increases the likelihood of adhesion, thereby contributing to higher roughness [61,62].

The influence of part geometry and surface remelting on surface roughness is clearly demonstrated in the work of Rombouts et al. [65]. Their study highlights how both the

shape of the component and the application of remelting strategies can significantly affect the final surface finish. The analyzed surface was the 0° up-skin, where the melt pool plays a key role in smoothing the surface. Their findings confirm that, under certain process parameters, the melt pool naturally contributes to reducing surface roughness. Moreover, applying a remelting strategy further enhances this effect, leading to even smoother surfaces.

Different up-skin surface angles, ranging from 15° to 75°, were analyzed in the same study. The results showed that as-built surface roughness increases with the inclination angle. However, applying a remelting strategy allows for reducing the roughness to values as low as 1.5 µm [65].

Layer thickness also contributes to the increase in surface roughness, due both to a larger melt pool—which increases the likelihood of melting loose powder on the surface—and to the staircase effect [63]. This is further influenced by the scan pattern, as studied by Ribeiro et al. on SS316L, who identified the Contour method as the most effective in achieving superior surface roughness [64].

The layer height is directly linked to the melt pool, which is in turn influenced by the laser power. As with other additive manufacturing technologies, excessively high or low energy densities can lead to the formation of defects in the deposited material track. Therefore, identifying an optimal intermediate point is essential to achieve desirable surface roughness [66].

The following table (Table 4) summarizes the main trends that emerged from the aforementioned literature search:

Table 4. Effect of LMD processing parameters on the as-built surface.

Variables	Action	Effect	Physical Mechanisms Involved
$\dot{V}_{CG}/\dot{V}_{SG}$	Increase	Increase track stability	Melt pool behavior
Particle size	Increase	Increase roughness	Melt pool behavior
$\dot{m}_p$	Increase	Increase roughness	Melt pool behavior
$\dot{V}_{SG}$ small particles	Increase	Not relevant	Not relevant
$\dot{V}_{SG}$ large particles	Increase	Roughness: Minimum at the extremes and central maximum	Dispersive powder
Surface remelting	Increase energy density	Decrease roughness	Reduce defects
Surface angles (Up-skin)	From 0° to 90°	Increase roughness	Staircase effect
Layer height	Increase	Increase roughness	Staircase effect

2.6. Wire Laser Energy Deposition

As with LMD technology, surface roughness in WLED varies depending on multiple factors and can be categorized into two types:

- Overall roughness, which accounts for the valleys between layers and the scan pattern tracks.
- Single-track roughness, which refers to the roughness measured only on the top surface of an individual track, is shaped by the melt pool after solidification.

Overall roughness is primarily influenced by geometric variables such as surface angle, layer thickness, and wire diameter [67].

The key process parameters affecting roughness include spot diameter, laser pulse rate and duration, wire feed angle, wire feed direction [68], wire feed rate, average laser power, and stage speed.

Shaikh et al. [67] conducted their analysis on 304 and 316L steel wire by keeping all other parameters constant while varying three key factors for single track: average laser power, pulse duration, and stage speed, and just two for multilayer deposition, fixing stage speed. The influence of average power, pulse duration, and stage speed on the width and height of the deposition track is illustrated in the work of Shaikh et al., where the relevant variables are, respectively, the overlap of adjacent tracks and the geometry of the deposition of different surface angles. An increase in width and a decrease in height is recorded with an increase in laser power and pulse duration, while an increase in stage speed reduces the height of the welding bead but almost does not affect the width.

Concerning overlap, ranging from 30% to 80% in 10% increments, it affects the continuity and uniformity of the surface, thereby influencing the final roughness. Results show that overlapping multiple tracks shows an improvement of surface finishing, reaching a maximum for 70% overlap, but then a drastic increase in roughness at 80% is observed. The effect of the deposition angles is also analyzed, with a maximum in roughness at 30° and lower values for 0° and 90° [24,67].

The feeding direction has a significant impact on surface roughness. Findings by Syed and Li indicate that when the wire approaches the melt pool from the front (front feeding), the resulting roughness is considerably lower compared to rear feeding. Furthermore, the angle at which the wire enters the melt pool also plays a role: in front feeding, roughness increases with the angle, whereas in rear feeding, the effect is reversed. These phenomena are primarily governed by the behavior of the melt pool and its cooling dynamics [68].

By comparing the studies conducted by Shaiki et al., Li et al., and Syed and Li, it becomes evident that the wire diameter directly affects the height of the weld bead and, consequently, the final surface roughness of the part. Specifically, an increase in wire diameter leads to a corresponding increase in roughness.

In the best cases, average surface roughness (Ra) values of approximately one micron were measured.

A study on the effect of auxiliary heating conducted by Sang et al. on stainless steel 304. The study analyzes the influence of both print bed and wire preheating on surface roughness. The roughness measured under auxiliary heating conditions was lower than that observed without heating. The investigated effect appears to contribute significantly to the reduction in defects and control of the melt pool cooling. The results obtained in this study were based on a lower laser power compared to other works, which may lead to defects that are subsequently mitigated by substrate and wire heating, providing additional energy to the material through alternative mechanisms [69].

The following table (Table 5) summarizes the main trends that emerged from the literature search:

Table 5. Effect of WLED processing parameters on the as-built surface.

Variables	Action	Effect	Physical Mechanisms Involved
Average Laser power	Increase	Increase width, decrease height of track	Melt pool behavior
Pulse duration	Increase	Increase width, decrease height of track	Melt pool behavior
Stage speed	Increase	Decrease width, decrease height of track	Melt pool behavior
Overlap	Increase	Roughness: Decrease with minimum at 70% then drastically increase at 80%	Partial remelting, remove defects
Deposition angles	From 0° to 90°	Roughness: Minimum at the extremes and central maximum	Melt pool behavior with gravity
Wire diameter	Increase	Increase roughness	Melt pool dimension
Alternative heating	Increase	Decrease roughness	Melt pool behavior

2.7. Wire Electron Beam Energy Deposition

To date, this technology has not been extensively investigated regarding surface roughness. Given the similarity of its machine architecture to that of WLED and WLAM systems [70], it is reasonable to expect that the roughness behavior may follow comparable trends. Parameters such as overlap and average power are likely to influence surface roughness in a similar manner, at least in the context of a single-track scan.

Electron beam power has been shown to have a similar effect to laser power on the width and height of welding beads [24].

However, surface roughness has scarcely been investigated in this context. To date, only the study by Kovalchuk reports roughness measurements, with values ranging between 0.3 and 1 mm [71].

2.8. Wire Arc Additive Manufacturing

Among all Arc-based DED technologies, Wire Arc Additive Manufacturing (WAAM) is the most widely adopted. It stands out for its simplicity and ranks among the fastest in terms of deposition rate. Similar to WLED and WEBAM, the surface topography in WAAM is influenced by the height and width of the single-track bead. The use of an electric arc introduces current (amperage) as an additional process parameter affecting surface roughness, alongside scan speed and wire feed rate, both of which also influence the geometry of the deposited bead.

For instance, in the case of stainless steel 316L, roughness values measured on single-track beads range from 1.00 to 8.32 μm [61].

When considering a complete component manufactured via WAAM, surface roughness tends to increase significantly due to the deposition pattern and the inherent layer-by-layer nature of the process. The accumulation of successive weld beads and the resulting stair-step effect contribute to a more pronounced surface irregularity compared to single-track measurements [72].

The overall surface topography is not determined anymore by the roughness alone [73]. The overall surface profile is predominantly influenced by waviness rather than micro-scale roughness. The maximum amplitude of these surface undulations ranges between 1.12 mm and 2.13 mm. These values are attributed to the presence of waves, bulges, and randomly occurring overlapping weld metal, which collectively contribute to the irregular surface morphology.

In WAAM technologies, inter-layer temperature is a key factor influencing surface roughness. Studies by Xiong et al. and Belhadj et al. have demonstrated a correlation whereby surface roughness increases with higher temperatures and decreases with increased travel speed. Consequently, longer deposition intervals between successive layers allow the previously deposited layer to cool down, resulting in reduced surface roughness [74,75].

Whenever an increase in a process variable leads to a rise in layer height, a corresponding increase in surface roughness is also observed. Modifying either the wire feed speed or the travel speed—while keeping the other constant—affects the resulting layer height. Specifically, increasing the travel speed reduces the layer height and consequently the surface roughness. Conversely, increasing the wire feed speed results in a higher layer height, which is associated with increased surface roughness [74].

The following table (Table 6) summarizes the main trends that emerged from the literature search:

Table 6. Effect of WAAM processing parameters on the as-built surface.

Variables	Action	Effect	Physical Mechanisms Involved
Wire feed rate	Increase	Increase bead height, decrease width, decrease wetting angle	Melt pool behavior
Wire feed rate	Increase	Increase roughness	Melt pool size
Travel speed	Increase	Decrease bead width, decrease melt through depth	Melt pool behavior
Travel speed	Increase	Decrease roughness	Melt pool size
Current	Increase	Roughness: Slight increase and then decrease	Melt pool behavior
Current	Increase	Increase bead width, increase melt through depth	Melt pool behavior
Layer height	Increase	Increase roughness	Melt pool size

2.9. Submerged Arc Additive Manufacturing

Like WAAM, the overall surface topography of components produced via SAAM is not solely defined by surface roughness but also significantly influenced by waviness. Waviness is closely related to the height and width of the single-track bead.

As SAAM is still an emerging technology, there is currently a lack of direct data regarding its surface topography. However, based on similarities with other arc-based processes—such as comparable deposition rates, layer thicknesses, and materials—it is reasonable to assume that the resulting waviness is of the same order of magnitude as that observed in WAAM. Therefore, the expected surface undulations can be estimated to fall within the millimeter range.

Current research on this technology continues to focus primarily on its mechanical properties, while surface finish remains largely unexplored. One advantage supporting these studies is that the deposition rate of this technology is even higher than that of WAAM. Moreover, components are rarely used in their as-built condition and are typically subjected to post-processing through machining [76,77].

2.10. Rapid Plasma Deposition

Like WAAM and SAAM, this technology is characterized by pronounced surface waviness, primarily due to its high layer thickness (3–4 mm) and elevated deposition rate [78].

As a relatively recent and patented process, there is currently a limited number of publications available on this research specifically addressing the ‘as-built’ surface characteristics. The same considerations and conclusions drawn for SAAM—regarding the influence of process parameters on surface topography—can be reasonably extended to Rapid Plasma Deposition (RPD) as well [79].

Nonetheless, the study conducted by Kumar and Jain provides a comprehensive overview of the process parameters and their influence on surface roughness. This study investigates the effect of power supply, travel speed, and metal feed rate on surface roughness for both powder- and wire-based technologies, specifically in the deposition of Stellite-6 onto an AISI 4130 steel substrate. Surface roughness exhibits a similar trend with respect to changes in process variables for both powder- and wire-based feedstock materials. As observed in previous technologies, increasing the travel speed and decreasing the material feed rate led to a reduction in surface roughness, primarily due to changes in layer height; meanwhile, an increase in the supplied power leads to a corresponding increase in surface roughness. Within the examined range of values, no plateau or maximum/minimum point is observed. The measured roughness values of 118 and 227 μm may still increase

or decrease depending on the influencing variables [80]. The following table (Table 7) summarizes the main trends that emerged from the above-mentioned literature search:

Table 7. Effect of RPD processing parameters on the as-built surface.

Variables	Action	Effect	Physical Mechanisms Involved
Laser power	Increase	Increase roughness	Melt pool behavior
Metal feed rate	Increase	Increase roughness	Melt pool size
Travel speed	Increase	Decrease roughness	Melt pool size

2.11. Cold Spray Additive Manufacturing

Since CSAM is a "cold" technology, the most suitable materials are ductile ones, which can deform and adhere effectively to the deposition surface, such as aluminum and copper [81,82]; nevertheless, steels, titanium, and nickel alloys can also be employed under suitable conditions [83,84].

The surface roughness is primarily influenced by particle diameter, gas temperature, and gas pressure. These parameters directly affect the particle velocity and deformation behavior upon impact, which in turn determine the quality of the deposited surface. Shao et al. [85] used a D10 = 9.11 µm, D50 = 20.9 µm, and D90 = 44.0 µm copper powder for their study. The two variables that have been investigated are pressure and temperature. These two ranged between 600 to 900 °C and from 4 to 5.5 MPa.

The average surface roughness (Ra) of cold-sprayed coatings was observed to decrease progressively with increasing gas pressure and gas temperature. In the study by Shao et al., Ra values ranged from 12.69 µm to 7.05 µm under varying process conditions [85].

The influence of particle size on surface roughness becomes evident when comparing these results with those reported by Sirvent et al. and similarly to Prashar and Vasudev [84,86], who employed larger particles and observed different roughness characteristics. Aluminum powder (indicated as Al-) used for their study has a D10 = 21.4 µm, D50 = 51.1 µm, and D90 = 100.3 µm, while the Titanium powder (indicated as Ti-) has a D10 = 8.5 µm, D50 = 24.8 µm, and D90 = 81.4 µm.

The sidewalls of components manufactured via Cold Spray exhibit surface waviness that significantly affects the overall topography, similarly to what has been observed in other additive technologies. These undulations are typically the result of cumulative deposition irregularities and process dynamics, and they contribute to a more complex surface morphology beyond micro-scale roughness alone.

Two scan strategies have been studied to analyze the effect on waviness: -T, traditional scan strategy, and -MK, metal knitting. The waviness parameter resulted in 531 ± 70 µm for the Al-MK sample and 296 ± 85 µm for the Ti-MK sample, whereas the -T samples did not exhibit such a marked difference. Similarly, surface roughness (Ra) values were comparable between aluminum and titanium samples, with approximately 70 µm for the MK samples and around 20 µm for the T samples [86].

The deposition of thick layers, as described by Prashar and Vasudev, leads to an increase in surface roughness, which correlates with waviness. Furthermore, deposits exceeding 1.5 mm in thickness exhibit low mechanical strength, necessitating both thermal and mechanical post-processing treatments [84].

The following table (Table 8) summarizes the main trends that emerged from the above-mentioned literature search:

Table 8. Effect of CSAM processing parameters on the as-built surface.

Variables	Action	Effect	Physical Mechanisms Involved
Particle diameter	Increase	Increase surface waviness	Interparticle defects
Gas temperature	Increase	Decrease roughness	Thermal energy involved in particle deformation
Gas pressure	Increase	Decrease roughness	Kinetic energy involved in particle deformation
Particle distribution-T	Increase	Not relevant	Not relevant
Particle distribution-MK	Increase	Increase surface waviness	Deposition strategy

2.12. Metal Binder Jetting

Like other additive manufacturing technologies, Binder Jetting is influenced by a variety of process parameters. Key variables include [29,87,88]:

- Layer thickness directly affects the overall surface topography.
- Printing speed of recoat is higher, where higher speeds may compromise dimensional accuracy and resolution.
- Roller rotation speed affects the powder flowability.
- Binder drops in size, as larger droplets tend to reduce surface resolution and detail.
- Binder saturation.
- Binder drying time.
- Powder characteristics, including particle size and spreading behavior, influence not only surface roughness but also internal porosity.

The interplay of these parameters plays a critical role in determining the final quality and performance of the printed component [29,87,88].

Powder size in Metal Binder Jetting (MBJ) can vary significantly depending on the application and desired resolution. While MBJ is compatible with fine powders typically used in Metal Injection Molding (MIM), it can also accommodate coarser powders. For instance, the study by Ziaee and Crane reports the use of powders with particle sizes exceeding 70 µm of many materials and alloys, such as K418 Nickel Superalloy and Copper. Such variations in powder size can influence not only the surface finish and resolution but also the packing density and final porosity of the printed parts [29,89].

Powder flowability can be managed with the Roller Rotation Speed, which help with powder flow and distribution, as Lores et al. findings show that, although to a lesser extent, it reduces surface roughness by improving powder packing [90].

There is currently limited research specifically addressing the influence of process parameters on surface roughness in Metal Binder Jetting (MBJ). While some studies suggest correlations, quantitative data remain scarce. One of the few detailed investigations is provided by Mostafaei et al. [91], who examined Inconel 625 using powder sizes ranging from 16 to 63 µm. The process parameters included a layer thickness of 100 µm, a recoat speed of 130 mm/s, a roller speed of 250 rpm, a roller traverse speed of 15 mm/s, and a drying speed of 17 mm/s. After sintering, the surface roughness resulted in having a root-mean-square height (Hrms) of 24.77 $\pm$ 5.13 µm, an Rq of 1.39 $\pm$ 0.2 µm, and an Ra of 1.10 $\pm$ 0.16 µm. Noticeably, the sintering process applied also affects such results.

The drying time of the binder is also a critical variable, as it not only contributes to increased surface roughness but also negatively affects the material's density. This is due to crack formation, which after prolonged drying periods, grows, and as a result, voids may form within the material, hindering the sintering process. A similar effect is caused by binder saturation. Insufficient binder leads to powder detachment, which in turn increases both surface roughness and porosity [90].

The following table (Table 9) summarizes the main trends that emerged from the above-mentioned literature search:

Table 9. Effect of MBJ processing parameters on the as-built surface.

Variables	Action	Effect	Physical Mechanisms Involved
Layer thickness	Increase	Increase roughness	Staircase effect
Particle size	Increase	Increase roughness	Lose resolution
Binder drops size	Increase	Increase roughness	Lose resolution
Printing speed/Recoating	Increase	Increase roughness	Binder drops drag
Surface angles	From 0° to 45°	Increase roughness	Staircase effect
Dring time	Increase	Increase roughness	Powder detachment
Binder saturation	Increase	Decrease roughness	Proper powder binding
Roller rotation speed	Increase	Decrease roughness	Proper powder flowability

2.13. Mold Slurry Deposition

Mold Slurry Deposition is an additive manufacturing technology patented by Tritone [30]. As a relatively recent development, it has not yet been extensively studied in terms of surface roughness on metallic materials. Due to its slurry-based process, it is widely used for ceramics, precious metals, and oxides [92–95]. The technique requires debinding and sintering, but the binder is highly robust, allowing for machining of the 'green' part prior to sintering. The wax mold not only defines the geometry of each individual layer but also serves as a support structure. As this is also layer-by-layer technology, it can be expected that surface roughness will depend on both layer thickness and the inclination of the surface relative to the build platform, but due to the lack of available references, the table reporting the effects of printing parameters on surface roughness will not be compiled.

2.14. Lithography-Based Metal Manufacturing

Like Metal Binder Jetting, the roughness in Lithography-based Metal Manufacturing (LMM) is influenced by key parameters that shape the component's topography. These include layer thickness, powder particle size, and the resolution of the Digital Light Processing (DLP) system—the component of the machine responsible for projecting the UV image that initiates polymerization of the powder—resin mixture [96]. Working with powders dispersed in a slurry/binder allows the use of finer particles and enables a reduction in layer thickness, with lower risks compared to the use of loose powders as in PBF technologies [31]. This technology typically employs MIM-grade 316L powders, such as those used in the study by Melentiev et al., with particle sizes ranging from 5 to 22 µm. The resulting surface roughness, measured across the entire surface, yielded a Sa value of 5.6 µm. High precision applications show an average surface roughness Ra of 1.6 µm [97,98].

The study by Mitteramskogler et al. highlighted how the inclination of the surface relative to the build plate affects surface roughness. A minimum roughness was observed for surfaces oriented either perpendicular or parallel to the build plate, while roughness significantly increased at small angles and then decreased again as the orientation approached vertical [99]. The following table (Table 10) summarizes the main trends that emerged from the above-mentioned literature search:

Table 10. Effect of LMM processing parameters on the as-built surface.

Variables	Action	Effect	Physical Mechanisms Involved
Layer thickness	Increase	Increase roughness	Staircase effect
Particle size	Increase	Increase roughness	Lose resolution
Surface angle	Minimum at 0° al 90°	Increase roughness	Staircase effect

2.15. Metal Material Jetting

MMJ can employ sub-micrometric powders suspended in the binder, allowing the printed layer thickness to be reduced to below 10 microns. Although no specific studies on surface roughness for metallic material are currently available, it can be reasonably stated—from studies conducted on polymers—that reducing layer thickness improves surface approximation, thereby minimizing the staircase effect. Furthermore, the use of ultra-fine powders contributes to enhanced sintering performance [33]. In addition to layer thickness, surface inclination also shows a direct correlation with roughness, as analyzed in the study by Kumar and Kumar [100]. More in-depth studies on the behavior of surface roughness in relation to changes in printing parameters remain to be explored.

2.16. Material Extrusion Additive Manufacturing

Filament and pellet extrusion technologies share the same printing architecture; the primary distinction lies in the form of the raw material, namely filament versus pellets. Several process parameters influence the resulting surface roughness, including layer thickness, surface angle, nozzle temperature, and printing speed. These variables affect the quality of interlayer bonding and the precision of material deposition, ultimately shaping the surface topography of the printed component [101].

The influence of process parameters on average surface roughness (Ra) in filament and pellet extrusion technologies has been investigated by Boschetto et al. [40], both in the green and sintered states, using a 316L powder-filled wire. Their findings indicate that Ra does not exhibit a consistent trend when varying nozzle temperature, printing speed, or layer thickness at a fixed surface angle. However, in both green and sintered parts, Ra shows a proportional increase with the surface angle, highlighting its dominant role in shaping surface topography. Figure 2 summarizes graphically the main results obtained by the reduced models obtained by Boschetto et al., where the lines indicate the layer thickness (L), in mm, the printing head temperature (T) in °C, and the speed (V) in mm/s.

This plot suggests that the primary factor influencing surface roughness is the surface angle, and therefore, the geometry of the printed component itself. As the surface angle increases, so does the average roughness (Ra), regardless of other process parameters, highlighting the critical role of part design in determining surface quality.

Consistent findings have been reported in other studies, showing similar roughness values under comparable surface analysis conditions [102–106].

Another variable that can affect surface roughness is the debinding and sintering process. As shown in the work of Obadimu and Kourousis, issues arising during sintering can lead to surface-related defects such as increased roughness, warping, and balling [106].

The following table (Table 11) summarizes the main trends that emerged from the above-mentioned literature search:

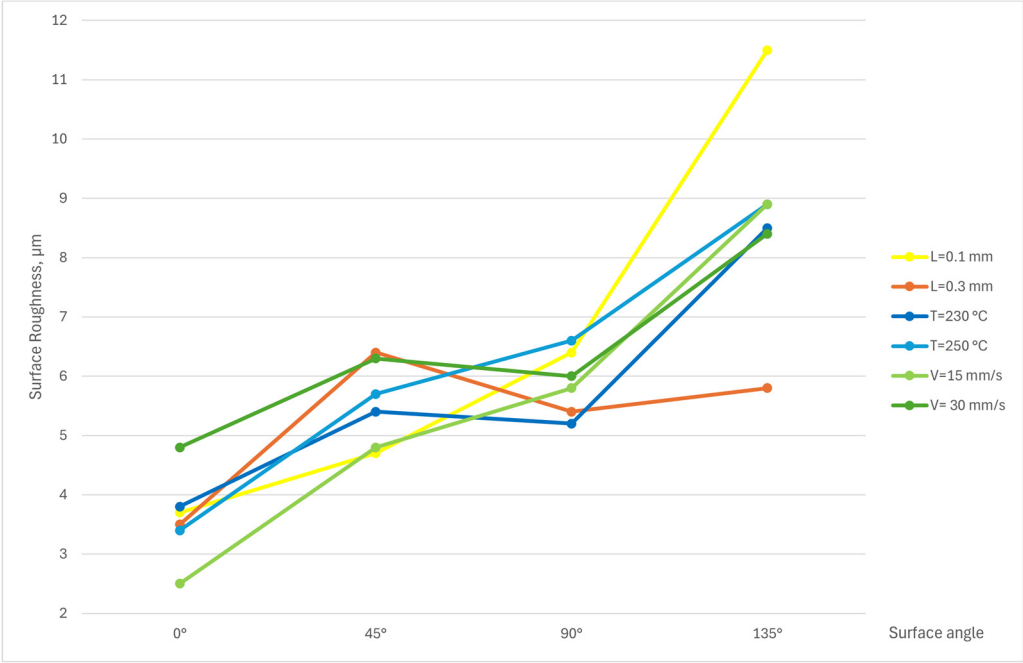

Figure 2. Ra value as a function of the surface angle for different printing parameters: L = layer thickness in mm, T = printing head temperature in °C, and V = head speed in mm/s.

Table 11. Effect of FDM processing parameters on the as-built surface.

Variables	Action	Effect	Physical Mechanisms Involved
Temperature	Increase	Different effects on different surface angles	Material deposition behavior
Deposition speed	Increase	Different effects on different surface angles	Material deposition behavior
Layer thickness	Increase	Different effects on different surface angles	Staircase effect
Surface angles	Increase	Increase roughness	Staircase effect

2.17. Dispersion Material Extrusion

The parameters that influence surface roughness in Direct Material Extrusion (DME) include extrusion thickness, extrusion width, printing speed, extrusion multiplier (a factor that adjusts the amount of extruded material, leading to over- or under-extrusion when this value is greater or less than 1), and finally, the particle size of the feedstock [35,107].

The parameter that most significantly affects surface roughness is the extrusion multiplier. When set too low, it leads to gaps between extrusion passes due to under-extrusion. Conversely, when set too high, it causes over-extrusion defects, resulting in a substantial increase in surface roughness. The Ra value measured in the worst case was 72 µm. Extrusion thickness ranks second in terms of its influence on surface roughness. Affecting the geometry of the deposited bead, it has a direct impact on the surface topography. This effect could potentially be amplified when considering inclined angles on the printed surface. Printing speed and bead width have the least influence on surface roughness. An increase in printing speed tends to raise roughness, as depositing a new layer onto a substrate where the binder has had time to dry results in fewer deformations. While increasing the bead width generally leads to a reduction in roughness, if the extruder is wider than the bead itself, positioning defects may occur [35,107].

An improvement in surface roughness was observed when sintering was performed under vacuum conditions. The best recorded Ra value was 18.59 microns [35,108].

The following table (Table 12) summarizes the main trends that emerged from the above-mentioned literature search:

Table 12. Effect of DME processing parameters on the as-built surface.

Variables	Action	Effect	Physical Mechanisms Involved
Extrusion thickness	Increase	Increase roughness when too high or too low	Material deposition behavior
Extrusion width	Increase	Decrease roughness	Decrease positioning defects
Printing speed	Increase	Increase roughness	Material deposition behavior
Extrusion multiplier	Increase	Increase roughness when too high or too low	Creating and filling void
Powder size	Increase	Decrease roughness	Increased sinterability

2.18. Laminate Layer Manufacturing

In LLM, surface roughness is influenced by both the layer thickness and the surface angle. This is due to the inherent roughness of the metal sheets used, which is typically characterized along the 0° and 90° orientations. As illustrated in Ahn et al. [109], surface roughness increases with layer thickness, a trend attributable to the layer-by-layer nature of the process. The roughness values measured in this study ranged from 2.09 µm to 75 µm, highlighting the significant impact of material and process parameters on the final surface quality. These values increase with a thicker layer. Due to the way the samples are made, in 0° and 180°, the roughness is the same as the stock material, and in 90°, the roughness is given by the cutting finishing [41]. The following table (Table 13) summarizes the main trends that emerged from the above-mentioned literature search:

Table 13. Effect of LLM processing parameters on the as-built surface.

Variables	Action	Effect	Physical Mechanisms Involved
Layer thickness	Increase	Increase roughness	Staircase effect
Base material roughness	Increase	Increase roughness	Direct exposure

2.19. Friction Energy Deposition

In FED, surface roughness can only be measured on the top surface parallel to the build platform, as the vertical walls formed during the process are significantly jagged. As a result, any functional application is not feasible without any kind of post-processing. This technology is therefore not suitable for producing near-net-shaped components [110].

The variables influencing surface roughness include the rotational speed of the tool, the feed rate, and the geometry of the tool head—specifically, the part responsible for generating heat through friction [111].

An increase in the rotational speed of the tool results in higher temperatures, which promotes the plasticization of the deposited material, improving its flow and thereby reducing surface roughness. Conversely, increasing the feed rate while maintaining the same rotational speed leads to lower temperatures, which in turn cause an increase in surface roughness [36,111]. The grooves on the tool head are believed to provide greater friction compared to a flat head, thereby generating more heat under identical movement and rotational speeds. However, the study does not offer a definitive conclusion regarding the optimal geometry of the tool [111]. The following table (Table 14) summarizes the main trends that emerged from the above-mentioned literature search:

Table 14. Effect of FED processing parameters on the as-built surface.

Variables	Action	Effect	Physical Mechanisms Involved
Tool geometry	Change	Grooves and rings on the surface	Increase heat generated by friction
Tool rotational speed	Increase	Decrease roughness	Increase temperature
Tool travel speed	Increase	Increase roughness	Decrease temperature

2.20. Drop-on-Demand Liquid Metal Jetting

In DOD-LMJ, the deposition process is characterized by a high-frequency release of discrete molten metal droplets, enabling precise control over material placement. The spatial arrangement of deposited droplets significantly affects the resulting surface topography. Gao et al. conducted a study analyzing its impact under four distinct droplet placement methodologies [112]. Even without changing the droplet distribution method, the spacing between droplets significantly affects surface roughness. For smaller droplets, roughness decreases as the spacing is reduced. In contrast, larger droplets may lead to flow inconsistencies, resulting in the formation of discontinuous lines and surface defects [113,114].

Another variable that significantly affects surface roughness is the substrate temperature. A higher substrate temperature prolongs the cooling time of the droplets, allowing the material to flow more effectively into surface pores and resulting in greater material densification and lower surface roughness [112,113].

However, the variable that most strongly influences surface roughness and morphology is the size of the individual droplets. By comparing the studies conducted by Gao et al., Lass et al., Simonelli et al., Traxel et al., and Watkins et al., it becomes evident that larger droplets lead to increased roughness. Due to the fact that, once solidified, larger droplets tend to form deeper valleys between them compared to smaller ones [40,112–115].

The average surface roughness, Ra, reported in these studies ranges from an optimal value of 4.62 µm up to 140 µm. The following table (Table 15) summarizes the main trends that emerged from the above-mentioned literature search:

Table 15. Effect of DOD-LMJ processing parameters on the as-built surface.

Variables	Action	Effect	Physical Mechanisms Involved
Drop arrangement	Change	Decrease roughness	Better drop positioning
Drop distance	Increase	Increase roughness	Deep valley formation
Substrate temperature	Increase	Decrease roughness	Slower cooling
Drop size	Increase	Increase roughness	Deep valley formation

3. Conclusions

Nearly all the cited studies on surface roughness have evaluated it using the average roughness parameter ‘Ra’. Only a few works have reported additional values such as ‘Rz’, ‘Sa’, and ‘Sz’, and even fewer have included other roughness metrics. Given the aim of this review as a guideline for global analysis and machine selection based on surface roughness, and considering the industry’s predominant demand for Ra, the conclusions will refer exclusively to this parameter. This choice is also due to the impracticality of providing inclusive results for all technologies discussed.

Metal Additive Manufacturing offers different processes, each one presenting its peculiarities and capabilities. This review addressed the process capabilities of the most used Metal AM techniques, in terms of surface quality in the as-built state, estimated by the average surface roughness, Ra. Even though the usefulness of Ra to assess the effective surface quality is highly debated, it is here taken as a reference to provide useful guidelines

on how to modify process parameters to control the average surface roughness. All the previous Tables describe the trends reported in literature for certain classes of materials and technologies, suggesting the effect of a single parameter on the resulting Ra. However, the literature search indicated synergistic effects of the parameters many times, as described in the text for the available examples; hence, the trends indicated in the tables should be taken only as a starting point for a multi-parameter optimization. In conclusion, Figure 3 reports the Ra values associated with each technology, highlighting that some encompass multiple effects and measurement conditions, while others refer to roughness values obtained solely on surfaces parallel to the build plane—that is, under more favorable conditions compared to the former. The blue arrows in Figure 3 highlight regions exhibiting surface roughness levels that exceed the scale represented in the graph. The reported maximum roughness values may be exceeded under more extreme printing conditions.

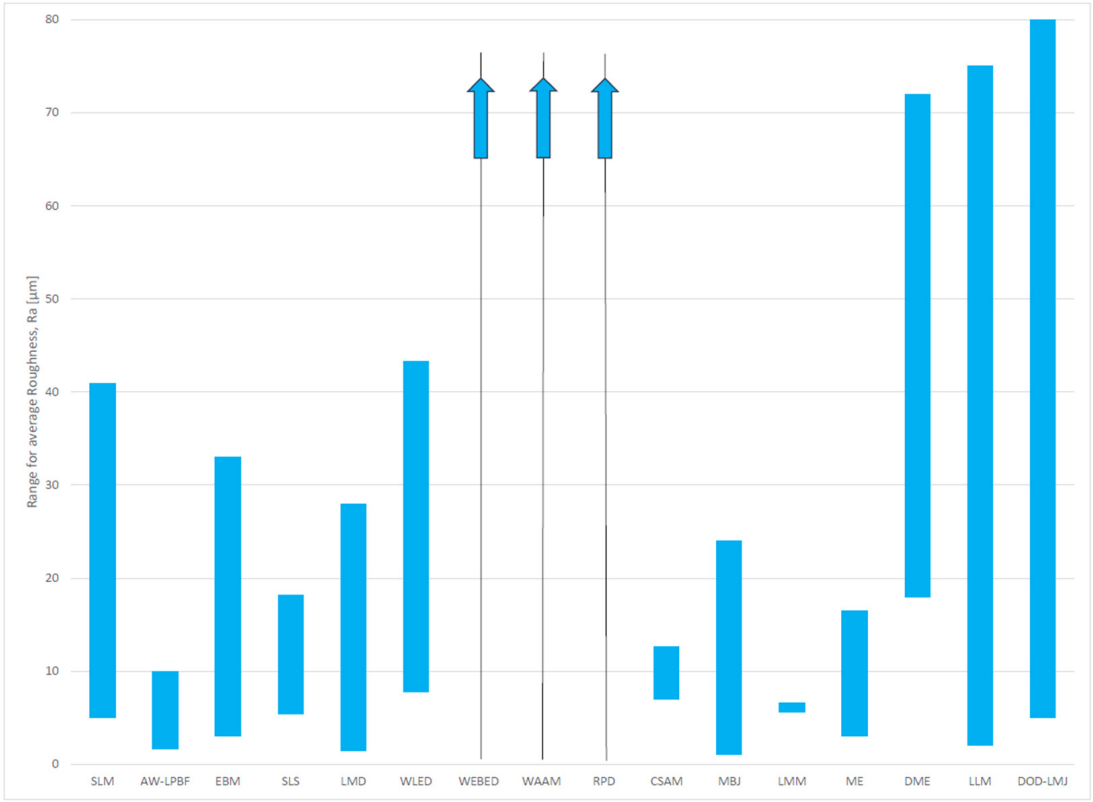

Figure 3. Range of the average roughness (Ra) for each of the reviewed technologies, presenting available data.

This review has also highlighted how printing parameters can lead to contrasting results across different studies, even when not limited to variations in materials. The conditions related to energy density proved to be decisive in this regard, showing that even when printing parameters are varied in the same way, the resulting surface roughness can differ significantly depending on the energy density levels.

Future research should aim at a more in-depth analysis of additional surface roughness parameters, while also expanding the scope to include all available printing materials and considering the influence of energy density. Moreover, some studies have focused solely on the roughness of the top surface parallel to the build plane. Given that additive manufacturing is inherently a layer-by-layer process and considering the strong influence of surface inclination, the use of test specimens printed with inclined surfaces, both in up-skin and down-skin orientations, to identify the critical angle beyond which the technology requires support structures, should be standardized and included in every research.

Author Contributions: Conceptualization, S.P. and E.B.; methodology, S.P. and P.V.; software, S.P.; formal analysis, P.V.; investigation, S.P.; resources, E.B.; data curation, S.P.; writing-original draft preparation, S.P.; writing-review and editing, P.V.; visualization, S.P.; supervision, P.V.; project administration, E.B.; funding acquisition, E.B. All authors have read and agreed to the published version of the manuscript.

Funding: This research received no external funding.

Data Availability Statement: No new data were created or analyzed in this study. Data sharing is not applicable to this article.

Conflicts of Interest: Author Enrico Bedogni was employed by the company Kosme s.r.l. Unipersonale. The remaining authors declare that the research was conducted in the absence of any commercial or financial relationships that could be construed as a potential conflict of interest.

Abbreviations

The following abbreviations are used in this manuscript:

AM	Additive Manufacturing
PBF	Powder Bed Fusion
DED	Direct Energy Deposition
BJ	Binder Jetting
ME	Material Extrusion
SLM	Selective Laser Melting
AWLPBF	Area Wise Laser Powder Bed Fusion
DiAM	Diode-based Additive Manufacturing
EBM	Electron Beam Melting
LMD	Laser Metal Deposition
LENS	Laser-Engineered Net Shaping
PLED	Powder Laser Energy Deposition
WLED	Wire Laser Energy Deposition
WLAM	Wire Laser Additive Manufacturing
WEBED	Wire Electron Beam Energy Deposition
WEBAM	Wire Electron Beam Additive Manufacturing
EBF^3	Electron Beam Freeform Fabrication
EBWFAM	Electron Beam Wire-Feed Additive Manufacturing
WAAM	Wire Arc Additive Manufacturing
GMAW	Gas Metal Arc Welding
SAAM	Submerged Arc Additive Manufacturing
RPD	Rapid Plasma Deposition
WPAED	Wire Plasma Arc Energy Deposition
PMD	Plasma Metal Deposition
GTAW	Gas Tungsten Arc Welding
MPA	Metal Powder Application
CSAM	Cold Spray Additive Manufacturing
MBJ	Metal Binder Jetting
MSD	Mold Slurry Deposition
MJ	MoldJet
LSD	Layerwise Slurry Deposition
LMM	Lithography-based Metal Manufacturing
DLP	Digital Light Processing
VPP	Vat Photo Polimerization
AWVP	Area Wise Vat Polimerization

UV	Ultraviolet
MJ	Material Jetting
MMJ	Metal Material Jetting
FDM	Fused Deposition Modeling
FME	Filament Material Extrusion
FFF	Fused Filament Fabrication
PME	Pellet Material Extrusion
DME	Dispersion Material Extrusion
LLM	Laminate Layer Manufacturing
SL	Sheet Lamination
FED	Friction Energy Deposition
FSAM	Friction Stir Additive Manufacturing
FSPAM	Friction Stir Powder Additive Manufacturing
AFSD	Additive Friction Stid Deposition
LMP	Liquid Metal Printing
DMW	Direct Metal Writing
DOD-LMJ	Drop-On-Demand Liquid Metal Jetting
MMJ	Molten Metal Jetting

References

1. Obilanade, D.; Dordlofva, C.; Törlind, P. Surface Roughness Considerations in Design for Additive Manufacturing-A Literature Review. *Proc. Des. Soc.* **2021**, *1*, 2841–2850. [CrossRef]
2. Afroz, L.; Qian, M.; Forsmark, J.; Li, Y.; Easton, M.; Das, R. Fatigue Life of Laser Powder Bed Fusion (L-PBF) AlSi10Mg Alloy: Effects of Surface Roughness and Porosity. *Prog. Addit. Manuf.* **2025**, *10*, 2423–2441. [CrossRef]
3. Cangussu, V.M.; Abrão, A.M.; Magalhães, F.d.C.; de Oliveira, D.A.; de Brito, P. The Influence of Deep Rolling on Surface Roughness, Corrosion Resistance and Fatigue Life of Annealed Aisi 1045 Steel. *Int J Adv Manuf Technol* **2025**, *139*, 4109–4124. [CrossRef]
4. Pagliari, L.; Gerosa, R.; Panzeri, D.; Fraccaroli, L.; Concli, F. High- and Low-Cycle Fatigue Behavior of Additively Manufactured Ti6Al4V and Influence of Surface Finish. *Eng. Fail. Anal.* **2025**, *180*, 109825. [CrossRef]
5. Perna, A.S.; Savio, L.; Coppola, M.; Scherillo, F. Investigating Fracture Behavior in Titanium Aluminides: Surface Roughness as an Indicator of Fracture Mechanisms in Ti-48Al-2Cr-2Nb Alloys. *Metals* **2025**, *15*, 49. [CrossRef]
6. Onafide, M.; Al Turk, A. Additive Manufacturing Techniques for Reducing Failure Modes and Enhancing Durability in Aerospace Components. *JMEI* **2025**, *18*, 42–52. [CrossRef]
7. Yin, T.; Miao, K.; Liu, H.; Fu, J. Contact and Wear Modelling of Rotary Seals under Mixed Lubrication in Piston Pumps for Aerospace Electro-Hydrostatic Actuators. *Chin. J. Aeronaut.* **2025**, *103575*. [CrossRef]
8. EHEDG: Guideline Catalogue. Available online: https://www.ehedg.org/guidelines-working-groups/guidelines/guidelines/guidelines/guidelines/detail/hygienic-design-principles (accessed on 14 September 2025).
9. Tian, X.; Li, T.; Liu, Y.; Tian, Y.; Li, Z.; Wang, Y.; Ma, Y.; Li, Y.; Wang, X.; Wang, W. Based on Surface Roughness and Hydrophobicity to Reduce the Bacterial Adhesion to Collagen Films for the Ability to Enhance the Shelf Life of Food. *Food Packag. Shelf Life* **2025**, *48*, 101473. [CrossRef]
10. Ihara, I.; Tokuda, H.; Schueller, J.K.; Mohamed, I.M.A.; Sakamoto, Y.; Toyoda, K.; Umetsu, K.; Yamaguchi, H. Surface Roughness and Cleanability: Evaluating the Impact of Magnetic Abrasive Finishing on Dairy Equipment. *J. Food Process Eng.* **2025**, *48*, e70106. [CrossRef]
11. Alsabti, M.A.; Ciuca, I.; Vasile, B.Ş.; Trusca, R.; Harb, A.A. The Effect of Surface Roughness and Hydroxyapatite Coating on the Biocompatibility of Co-Cr Alloys for Medical Implants. *Preprint* **2025**. [CrossRef]
12. Mathur, M.; Paliwal, N.; Kumar, S.; Kumar, K.; Gautam, S.K.; Jewariya, M. Texture Characterization of Bipolar Hip Joint Medical Implants Using Optical Methods. *MAPAN* **2025**, *40*, 471–476. [CrossRef]
13. Bharatish, A.; Kumar, A.; Siddhanth, K.S.; Manikant, V.; Jagdish, P.; Sharma, A.; Solaiachari, S. On Optimizing Wettability, Surface Roughness and Swelling Behaviour of Laser-Polished 3D-Printed PETG Polymer for Bio-Medical Implants. *Polymer* **2025**, *330*, 128482. [CrossRef]
14. Xu, R.; Jin, X.; Bi, H.; Zhang, Z.; Li, M. Effect of Surface Roughness on Contact Resistance and Electrochemical Corrosion Behavior of 446 Stainless Steel in Simulated Anode Environments for Proton Exchange Membrane Fuel Cell. *J. Solid State Electrochem.* **2024**, *28*, 3087–3098. [CrossRef]

15. Song, X.; Liu, F.; Yan, Y.; Wang, W.; Wang, Y.; Sun, W.; Cui, J. Influence of Surface Roughness of Thermal Barrier Coating on the Cooling Performance of a Film-Cooled Turbine Vane. *Case Stud. Therm. Eng.* **2025**, *65*, 105698. [CrossRef]
16. Heidarinejad, A.; Ashrafizadeh, F. Influence of Surface Texture and Coating Thickness on Adhesion of Nickel Plated Coatings to Aluminium Substrate. *J. Manuf. Process.* **2024**, *120*, 435–448. [CrossRef]
17. Ngo, T.D.; Kashani, A.; Imbalzano, G.; Nguyen, K.T.Q.; Hui, D. Additive Manufacturing (3D Printing): A Review of Materials, Methods, Applications and Challenges. *Compos. Part B Eng.* **2018**, *143*, 172–196. [CrossRef]
18. Sefene, E.M. State-of-the-Art of Selective Laser Melting Process: A Comprehensive Review. *J. Manuf. Syst.* **2022**, *63*, 250–274. [CrossRef]
19. Seurat | Area Printing | Metal Additive Manufacturing | 3D Printing. Available online: https://www.seurat.com/area-printing (accessed on 19 February 2025).
20. Murr, L.E.; Li, S. Electron-Beam Additive Manufacturing of High-Temperature Metals. *MRS Bull.* **2016**, *41*, 752–757. [CrossRef]
21. Kruth, J.; Mercelis, P.; Van Vaerenbergh, J.; Froyen, L.; Rombouts, M. Binding Mechanisms in Selective Laser Sintering and Selective Laser Melting. *Rapid Prototyp. J.* **2005**, *11*, 26–36. [CrossRef]
22. Ahn, D.G. Directed Energy Deposition (DED) Process: State of the Art. *Int. J. Precis. Eng. Manuf. Green Tech.* **2021**, *8*, 703–742. [CrossRef]
23. Graf, B.; Marko, A.; Petrat, T.; Gumenyuk, A.; Rethmeier, M. 3D Laser Metal Deposition: Process Steps for Additive Manufacturing. *Weld World* **2018**, *62*, 877–883. [CrossRef]
24. Ding, D.; Pan, Z.; Cuiuri, D.; Li, H. Wire-Feed Additive Manufacturing of Metal Components: Technologies, Developments and Future Interests. *Int. J. Adv. Manuf. Technol.* **2015**, *81*, 465–481. [CrossRef]
25. Treutler, K.; Wesling, V. The Current State of Research of Wire Arc Additive Manufacturing (WAAM): A Review. *Appl. Sci.* **2021**, *11*, 8619. [CrossRef]
26. Nickels, L. Additive Manufacturing: A User's Guide. *Met. Powder Rep.* **2016**, *71*, 100–105. [CrossRef]
27. Additive Manufacturing at HERMLE. Available online: https://www.hermle.de/en/additive-manufacturing/ (accessed on 25 February 2025).
28. Impact Innovations | Cold Spraying. Available online: https://impact-innovations.com/en/ (accessed on 3 March 2025).
29. Ziaee, M.; Crane, N.B. Binder Jetting: A Review of Process, Materials, and Methods. *Addit. Manuf.* **2019**, *28*, 781–801. [CrossRef]
30. Tritone Technologies. Available online: https://tritoneam.com (accessed on 21 February 2025).
31. Rieger, T.; Schubert, T.; Schurr, J.; Butschle, M.; Schwenkel, M.; Bernthaler, T.; Schneider, G. Slurry Development for Lithography-Based Additive Manufacturing of Cemented Carbide Components. *Powder Technol.* **2021**, *383*, 498–508. [CrossRef]
32. Gülcan, O.; Günaydın, K.; Tamer, A. The State of the Art of Material Jetting—A Critical Review. *Polymers* **2021**, *13*, 2829. [CrossRef]
33. Ibrahim, B.; Lopez, L.; Kulkarni, S.; Jobes, D.; Forgiarini, M.; Barber, J.R.; Gordon, J.V. Increasing Strength Properties in Sinter-Based Additive Manufacturing of SS316L via Metal Material Jetting of Sub-Micron Powders. *Addit. Manuf.* **2024**, *89*, 104268. [CrossRef]
34. Ramazani, H.; Kami, A. Metal FDM, a New Extrusion-Based Additive Manufacturing Technology for Manufacturing of Metallic Parts: A Review. *Prog. Addit. Manuf.* **2022**, *7*, 609–626. [CrossRef]
35. Hoffmann, M.; Elwany, A. Material Extrusion Additive Manufacturing of AISI 316L Pastes. *J. Manuf. Process.* **2023**, *108*, 238–251. [CrossRef]
36. Chen, L.; Lu, L.; Zhu, L.; Yang, Z.; Zhou, W.; Ren, X.; Zhang, X. Microstructure Evolution and Mechanical Properties of Multilayer AA6061 Alloy Fabricated by Additive Friction Stir Deposition. *Met. Mater. Trans. A* **2024**, *55*, 1049–1064. [CrossRef]
37. Hassan, A.; Pedapati, S.R.; Awang, M.; Soomro, I.A. A Comprehensive Review of Friction Stir Additive Manufacturing (FSAM) of Non-Ferrous Alloys. *Materials* **2023**, *16*, 2723. [CrossRef] [PubMed]
38. Abankar, M.; Lunetto, V.; De Maddis, M.; Russo Spena, P. Friction Stir Welding of Additively Manufactured A20X Aluminum Alloy: Welding Process, Mechanical Properties, and Microstructure. *Int. J. Adv. Manuf. Technol.* **2024**, *135*, 4635–4652. [CrossRef]
39. Elton, E.S.; Traxel, K.D.; Pascall, A.J.; Jeffries, J.R. Jet on Demand—A Pneumatically Driven Molten Metal Jetting Method for Printing Crack-Free Aluminum Components. *Addit. Manuf. Lett.* **2024**, *11*, 100240. [CrossRef]
40. Watkins, N.N.; Traxel, K.D.; Wilson-Heid, A.E.; Reeve, T.C.; Silva, C.M.; Jeffries, J.R.; Pascall, A.J. Process-Structure-Property Relationships for Droplet-on-Demand Liquid-Metal-Jetted Parts. *Addit. Manuf.* **2023**, *73*, 103709. [CrossRef]
41. Rice, C.S.; Mendez, P.F.; Brown, S.B. Metal Solid Freeform Fabrication Using Semi-Solid Slurries. *JOM* **2000**, *52*, 31–33. [CrossRef]
42. Ramachandramoorthy, R.; Kang, S.G. Process for the Manufacturing of Microscale Hollow Metal Bodies 2024. Available online: https://worldwide.espacenet.com/patent/search/family/083898424/publication/EP4357296A1?q=Exaddon%20ceres (accessed on 12 September 2025).
43. Microscale 3D Printing for Fundamental Research. Available online: https://www.exaddon.com/micro3d-research (accessed on 14 September 2025).
44. Ru, C.; Luo, J.; Xie, S.; Sun, Y. A Review of Non-Contact Micro- and Nano-Printing Technologies. *J. Micromech. Microeng.* **2014**, *24*, 053001. [CrossRef]

45. Mansoura, A.; Dehghan, S.; Barka, N.; Kangranroudi, S.S. Investigation into the Effect of Process Parameters on Density, Surface Roughness, and Mechanical Properties of 316L Stainless Steel Fabricated by Selective Laser Melting. *Int. J. Adv. Manuf. Technol.* **2024**, *130*, 2547–2562. [CrossRef]
46. Yildiz, R.A.; Ozdogan, C.; Malekan, M. On the Surface Roughness of 316L Stainless Steel Fabricated Using L-PBF Additive Manufacturing. *Finn. J. Trib.* **2024**, *41*, 54–56. [CrossRef]
47. Correa-Gómez, E.; Castro-Espinosa, H.; Caballero-Ruiz, A.; García-López, E.; Ruiz-Huerta, L. Effect of Process Parameters on the Roughness and Tensile Behavior of Parts Manufactured by the Metals LPBF Process. *Eng. Rep.* **2024**, *6*, e12904. [CrossRef]
48. Jiang, H.Z.; Li, Z.Y.; Feng, T.; Wu, P.Y.; Chen, Q.S.; Feng, Y.L.; Chen, L.F.; Hou, J.Y.; Xu, H.J. Effect of Process Parameters on Defects, Melt Pool Shape, Microstructure, and Tensile Behavior of 316L Stainless Steel Produced by Selective Laser Melting. *Acta Metall. Sin.* **2021**, *34*, 495–510. [CrossRef]
49. Wang, D.; Mai, S.; Xiao, D.; Yang, Y. Surface Quality of the Curved Overhanging Structure Manufactured from 316-L Stainless Steel by SLM. *Int. J. Adv. Manuf. Technol.* **2016**, *86*, 781–792. [CrossRef]
50. Sinico, M.; Witvrouw, A.; Dewulf, W. Influence of the Particle Size Distribution on Surface Quality of Maraging 300 Parts Produced by Laser Powder Bed Fusion. In Proceedings of the Special Interest Group meeting on Advancing Precision in Additive Manufacturing, Berlin, Germany, 6–9 October 2025; pp. 31–34.
51. Fotovvati, B.; Le, T.N.; Ferreri, N.; Shrestha, S.; Duanmu, N. Effects of Powder Characteristics of Different Alloy Powders on Part Quality in Area Printing® Additive Manufacturing. In *2024 International Solid Freeform Fabrication Symposium, Austin, TX, USA, 11-14 August 2024*; University of Texas at Austin: Austin, TX, USA, 2024.
52. Matthews, M.J.; Guss, G.; Drachenberg, D.R.; Demuth, J.A.; Heebner, J.E.; Duoss, E.B.; Kuntz, J.D.; Spadaccini, C.M. Diode-Based Additive Manufacturing of Metals Using an Optically-Addressable Light Valve. *Opt. Express* **2017**, *25*, 11788. [CrossRef]
53. Galati, M.; Minetola, P.; Rizza, G. Surface Roughness Characterisation and Analysis of the Electron Beam Melting (EBM) Process. *Materials* **2019**, *12*, 2211. [CrossRef]
54. Wang, P.; Sin, W.; Nai, M.; Wei, J. Effects of Processing Parameters on Surface Roughness of Additive Manufactured Ti-6Al-4V via Electron Beam Melting. *Materials* **2017**, *10*, 1121. [CrossRef] [PubMed]
55. Safdar, A.; He, H.Z.; Wei, L.; Snis, A.; Chavez De Paz, L.E. Effect of Process Parameters Settings and Thickness on Surface Roughness of EBM Produced Ti-6Al-4V. *Rapid Prototyp. J.* **2012**, *18*, 401–408. [CrossRef]
56. Wang, Y.; Bergström, J.; Burman, C. Characterization of an Iron-Based Laser Sintered Material. *J. Mater. Process. Technol.* **2006**, *172*, 77–87. [CrossRef]
57. Sachdeva, A.; Singh, S.; Sharma, V.S. Investigating Surface Roughness of Parts Produced by SLS Process. *Int. J. Adv. Manuf. Technol.* **2013**, *64*, 1505–1516. [CrossRef]
58. Song, Y.A.; Koenig, W. Experimental Study of the Basic Process Mechanism for Direct Selective Laser Sintering of Low-Melting Metallic Powder. *CIRP Ann.* **1997**, *46*, 127–130. [CrossRef]
59. Attarzadeh, F.; Fotovvati, B.; Fitzmire, M.; Asadi, E. Surface Roughness and Densification Correlation for Direct Metal Laser Sintering. *Int. J. Adv. Manuf. Technol.* **2020**, *107*, 2833–2842. [CrossRef]
60. Zhu, P.; He, X.; Guan, H.; Zhang, Z.; Zhang, T.; Qu, X. Study on Improving Properties of High-Density 316 L Stainless Steel Fabricated by Indirect Selective Laser Sintering. *Mater. Today Commun.* **2025**, *46*, 112496. [CrossRef]
61. Nuñez, L.; Downey, C.M.; Van Rooyen, I.J.; Charit, I.; Maughan, M.R. Analysis of Surface Roughness in Metal Directed Energy Deposition. *Int. J. Adv. Manuf. Technol.* **2024**. [CrossRef]
62. Jardon, Z.; Ertveldt, J.; Lecluyse, R.; Hinderdael, M.; Pyl, L. Directed Energy Deposition Roughness Mitigation through Laser Remelting. *Procedia CIRP* **2022**, *111*, 180–184. [CrossRef]
63. Gradl, P.R.; Cervone, A.; Gill, E. Surface Texture Characterization for Thin-Wall NASA HR-1 Fe–Ni–Cr Alloy Using Laser Powder Directed Energy Deposition (LP-DED). *Adv. Ind. Manuf. Eng.* **2022**, *4*, 100084. [CrossRef]
64. Ribeiro, K.S.B.; Mariani, F.E.; Coelho, R.T. A Study of Different Deposition Strategies in Direct Energy Deposition (DED) Processes. *Procedia Manuf.* **2020**, *48*, 663–670. [CrossRef]
65. Rombouts, M.; Maes, G.; Hendrix, W.; Delarbre, E.; Motmans, F. Surface Finish after Laser Metal Deposition. *Phys. Procedia* **2013**, *41*, 810–814. [CrossRef]
66. Yazar, K.U.; Pawar, S.; Park, K.S.; Choi, S.H. Effect of Process Parameters on the Clad Morphology, Microstructure, Microtexture, and Hardness of Single Layer 316 L Stainless Steel during Direct Energy Deposition. *Mater. Charact.* **2022**, *191*, 112148. [CrossRef]
67. Shaikh, M.O.; Chen, C.C.; Chiang, H.C.; Chen, J.R.; Chou, Y.C.; Kuo, T.Y.; Ameyama, K.; Chuang, C.H. Additive Manufacturing Using Fine Wire-Based Laser Metal Deposition. *RPJ* **2019**, *26*, 473–483. [CrossRef]
68. Syed, W.U.H.; Li, L. Effects of Wire Feeding Direction and Location in Multiple Layer Diode Laser Direct Metal Deposition. *Appl. Surf. Sci.* **2005**, *248*, 518–524. [CrossRef]
69. Sang, Y.X.; Xiao, M.Z.; Zhang, Z.J.; Fu, Q.Y. Effect of Auxiliary Heating Process on Low Power Pulsed Laser Wire Feeding Deposition. *Mater. Des.* **2022**, *218*, 110666. [CrossRef]

70. Metal 3D Printers | Metal 3D Printing Machines | Sciaky. Available online: https://www.sciaky.com/additive-manufacturing/industrial-metal-3d-printers (accessed on 8 September 2025).
71. Kovalchuk, D.; Melnyk, V.; Melnyk, I. A Coaxial Wire-Feed Additive Manufacturing of Metal Components Using a Profile Electron Beam in Space Application. *J. Mater. Eng. Perform.* **2022**, *31*, 6069–6082. [CrossRef]
72. Hensel, J.; Przyklenk, A.; Müller, J.; Köhler, M.; Dilger, K. Surface Quality Parameters for Structural Components Manufactured by DED-Arc Processes. *Mater. Des.* **2022**, *215*, 110438. [CrossRef]
73. Dinovitzer, M.; Chen, X.; Laliberte, J.; Huang, X.; Frei, H. Effect of Wire and Arc Additive Manufacturing (WAAM) Process Parameters on Bead Geometry and Microstructure. *Addit. Manuf.* **2019**, *26*, 138–146. [CrossRef]
74. Xiong, J.; Li, Y.; Li, R.; Yin, Z. Influences of Process Parameters on Surface Roughness of Multi-Layer Single-Pass Thin-Walled Parts in GMAW-Based Additive Manufacturing. *J. Mater. Process. Technol.* **2018**, *252*, 128–136. [CrossRef]
75. Belhadj, M.; Werda, S.; Kromer, R.; Darnis, P. Influence of Operating Parameters on the Mechanical and Geometric Properties of 316L Stainless Steel Structures Fabricated by WAAM-CMT. *Procedia CIRP* **2025**, *133*, 585–590. [CrossRef]
76. Li, Y.; Wu, S.; Li, H.; Dong, Y.; Cheng, F. Submerged Arc Additive Manufacturing (SAAM) of Low-Carbon Steel: Effect of in-Situ Intrinsic Heat Treatment (IHT) on Microstructure and Mechanical Properties. *Addit. Manuf.* **2021**, *46*, 102124. [CrossRef]
77. Cheng, F.; Xue, M.; Zhang, B.; Yan, S.; Wu, S. Submerged Arc Additive Manufacturing of Duplex Stainless Steel: Effect of Intrinsic Heat Treatment on Microstructure, Mechanical Properties and Pitting Resistance. *J. Mater. Process. Technol.* **2025**, *341*, 118885. [CrossRef]
78. Norsk Titanium | Technology. Available online: https://www.norsktitanium.com/technology#process (accessed on 5 May 2025).
79. Ariza-Galván, E.; Montealegre-Meléndez, I.; Pérez-Soriano, E.M.; Neubauer, E.; Kitzmantel, M.; Arévalo, C. Influence of Processing Conditions on the Mechanical Properties of 17-4PH Specimens Produced by Additive Manufacturing. *Machines* **2022**, *10*, 976. [CrossRef]
80. Kumar, P.; Jain, N.K. Surface Roughness Prediction in Micro-Plasma Transferred Arc Metal Additive Manufacturing Process Using K-Nearest Neighbors Algorithm. *Int. J. Adv. Manuf. Technol.* **2022**, *119*, 2985–2997. [CrossRef]
81. Wu, H.; Xie, X.; Liu, M.; Verdy, C.; Zhang, Y.; Liao, H.; Deng, S. Stable Layer-Building Strategy to Enhance Cold-Spray-Based Additive Manufacturing. *Addit. Manuf.* **2020**, *35*, 101356. [CrossRef]
82. Wang, X.; Feng, F.; Klecka, M.A.; Mordasky, M.D.; Garofano, J.K.; El-Wardany, T.; Nardi, A.; Champagne, V.K. Characterization and Modeling of the Bonding Process in Cold Spray Additive Manufacturing. *Addit. Manuf.* **2015**, *8*, 149–162. [CrossRef]
83. Vaz, R.; Garfias, A.; Albaladejo, V.; Sanchez, J.; Cano, I. A Review of Advances in Cold Spray Additive Manufacturing. *Coatings* **2023**, *13*, 267. [CrossRef]
84. Prashar, G.; Vasudev, H. A Comprehensive Review on Sustainable Cold Spray Additive Manufacturing: State of the Art, Challenges and Future Challenges. *J. Clean. Prod.* **2021**, *310*, 127606. [CrossRef]
85. Shao, L.; Xue, N.; Li, W.; Liu, S.; Tu, Z.; Chen, Y.; Zhang, J.; Dai, S.; Liu, Q.; Shi, X.; et al. Effect of Cold-Spray Parameters on Surface Roughness, Thickness and Adhesion of Copper-Based Composite Coating on Aluminum Alloy 6061 T6 Substrate. *Processes* **2023**, *11*, 959. [CrossRef]
86. Sirvent, P.; Lozano, A.; Garrido-Maneiro, M.A.; Poza, P.; Vaz, R.F.; Albaladejo-Fuentes, V.; Cano, I.G. Surface Topography Analysis in Cold Spray Additive Manufacturing. *Precis. Eng.* **2025**, *92*, 207–218. [CrossRef]
87. Mao, Y.; Li, J.; Li, W.; Cai, D.; Wei, Q. Binder Jetting Additive Manufacturing of 316L Stainless-Steel Green Parts with High Strength and Low Binder Content: Binder Preparation and Process Optimization. *J. Mater. Process. Technol.* **2021**, *291*, 117020. [CrossRef]
88. Myers, K.; Paterson, A.; Iizuka, T.; Klein, A. The Effect of Print Speed on Surface Roughness and Density Uniformity of Parts Produced Using Binder Jet 3D Printing 2021. *arXiv* **2021**, arXiv:2021010459. [CrossRef]
89. Fang, X.; Zu, Y.; Ma, Q.; Hu, J. State of the Art of Metal Powder Bonded Binder Jetting Printing Technology. *Discov. Mater.* **2023**, *3*, 15. [CrossRef]
90. Lores, A.; Azurmendi, N.; Agote, I.; Espinosa, E.; García-Blanco, M.B. A Study of Parameter and Post-Processing Effects on Surface Quality Improvement of Binder Jet 3D-Printed Invar36 Alloy Parts. *Prog. Addit. Manuf.* **2022**, *7*, 917–930. [CrossRef]
91. Mostafaei, A.; Neelapu, S.H.V.R.; Kisailus, C.; Nath, L.M.; Jacobs, T.D.B.; Chmielus, M. Characterizing Surface Finish and Fatigue Behavior in Binder-Jet 3D-Printed Nickel-Based Superalloy 625. *Addit. Manuf.* **2018**, *24*, 200–209. [CrossRef]
92. Vompe, T.; Goviazin, G.G.; Dolev, O.; Rudnik, L.; Katz-Demyanetz, A. Sintering of Additively Manufactured Zirconium by MoldJet Technology. *Powder Technol.* **2024**, *436*, 119494. [CrossRef]
93. Tian, X.; Mühler, C.; Günster, J.; Heinrich, J.G. Feasibility Study on Rapid Prototyping of Porcelain Products. *J. Ceram. Sci. Tech.* **2011**, *2*, 217–226. [CrossRef]
94. Addess, A.; Shilo, D.; Glass, B.; Paskovitch, Y.; Burkhardt, C.; Vogel, L.; Rabkin, E.; Faran, E. Additive Manufacturing of Ni–Ti SMA by the Sinter-Based MoldJet Method. *Shap. Mem. Superelasticity* **2025**, *11*, 89–99. [CrossRef]
95. Hoffmann, M.; Schubert, N.H.; Günster, J.; Stawarczyk, B.; Zocca, A. Additive Manufacturing of Glass-Ceramic Dental Restorations by Layerwise Slurry Deposition (LSD-Print). *J. Eur. Ceram. Soc.* **2025**, *45*, 117235. [CrossRef]

96. Harakaly, G.; Cano Cano, S.; Bosters, J.; Sperling, C.; Moedder, D.; Mitteramskogler, G. Recent Advances in the Biomedical Field with the Lithography-Based Metal Manufacturing Process. *J. Jpn. Soc. Powder Powder Metall.* **2025**, *72*, S1227–S1231. [CrossRef]
97. Melentiev, R.; Harakály, G.; Stögerer, J.; Mitteramskogler, G.; Wagih, A.; Lubineau, G.; Grande, C.A. High-Resolution Metal 3D Printing via Digital Light Processing. *Addit. Manuf.* **2024**, *85*, 104156. [CrossRef]
98. Melentiev, R.; Wagih, A.; Lagerweij, A.; Mitteramskogler, G.; Lubineau, G.; Grande, C.A. Unlocking Multiscale Metallic Metamaterials via Lithography Additive Manufacturing. *Virtual Phys. Prototyp.* **2024**, *19*, e2339368. [CrossRef]
99. Mitteramskogler, G.; Schwentenwein, M.; Burkhardt, C.; Cruchley, N. Lithography-Based Metal Manufacturing (LMM) of 316L Powder. Additive Manufacturing. Euro PM 2018 Congress and Exibition—Conference Paper—2020. Available online: https://sites.shocklogic.com/demos/portable_abstract_book/Euro%20PM2018%20Proceedings/EuroPM2018%20Proceedings/assets/3987667.pdf (accessed on 18 August 2025).
100. Kumar, K.; Kumar, G.S. A Study on Surface Roughness of Rapid Prototypes Fabricated Using Poly-Jet 3D Printing System. In Proceedings of the International Conference on Computer Aided Engineering (CAE 2013), Chennani, India, 19-21 December 2013; pp. 1–6.
101. Boschetto, A.; Bottini, L.; Miani, F.; Veniali, F. Roughness Investigation of Steel 316L Parts Fabricated by Metal Fused Filament Fabrication. *J. Manuf. Process.* **2022**, *81*, 261–280. [CrossRef]
102. Baligidad, S.M.; Chandra, B.T.; Girish, S.M. Fused Filament Fabrication of Stainless Steel 316L: Investigation on Effect of Printing Parameters on Microstructural and Mechanical Strength of Sintered Part. *IJSRP* **2024**, *14*, 242–255. [CrossRef]
103. Caminero, M.Á.; Romero Gutiérrez, A.; Chacón, J.M.; García-Plaza, E.; Núñez, P.J. Effects of Fused Filament Fabrication Parameters on the Manufacturing of 316L Stainless-Steel Components: Geometric and Mechanical Properties. *RPJ* **2022**, *28*, 2004–2026. [CrossRef]
104. Jacob, J.; Pejak Simunec, D.; Kandjani, A.E.Z.; Trinchi, A.; Sola, A. A Review of Fused Filament Fabrication of Metal Parts (Metal FFF): Current Developments and Future Challenges. *Technologies* **2024**, *12*, 267. [CrossRef]
105. Naim, M.; Chemkhi, M.; Alhussein, A.; Retraint, D. Effect of Post-Treatments on the Tribological and Corrosion Behavior of 17–4PH Stainless Steel Processed via Fused Filament Fabrication. *Addit. Manuf. Lett.* **2023**, *7*, 100158. [CrossRef]
106. Obadimu, S.O.; Kourousis, K.I. Shrinkage Behaviour of Material Extrusion Steel 316L: Influence of Primary 3D Printing Parameters. *RPJ* **2022**, *28*, 92–101. [CrossRef]
107. Utela, B.; Storti, D.; Anderson, R.; Ganter, M. A Review of Process Development Steps for New Material Systems in Three Dimensional Printing (3DP). *J. Manuf. Process.* **2008**, *10*, 96–104. [CrossRef]
108. Alaghmandfard, R.; Aghayar, Y.; Ester, D.; Mohammadi, M.; Borisoff, J.; Dotto, K. Sintering Process Optimization of the Additively Manufactured Pure Copper Parts through the Metal Paste Deposited Process. *J. Alloys Compd.* **2024**, *1009*, 176932. [CrossRef]
109. Ahn, D.; Kweon, J.H.; Choi, J.; Lee, S. Quantification of Surface Roughness of Parts Processed by Laminated Object Manufacturing. *J. Mater. Process. Technol.* **2012**, *212*, 339–346. [CrossRef]
110. Sharma, A.; Bandari, V.; Ito, K.; Kohama, K.; Ramji, M.; Himasekhar Sai, B.V. A New Process for Design and Manufacture of Tailor-Made Functionally Graded Composites through Friction Stir Additive Manufacturing. *J. Manuf. Process.* **2017**, *26*, 122–130. [CrossRef]
111. Chaudhary, B.; Jain, N.K.; Murugesan, J. Experimental Investigation and Parametric Optimization of Friction Stir Powder Additive Manufacturing Process for Aerospace-Grade Al Alloy. *Int. J. Adv. Manuf. Technol.* **2022**, *123*, 603–625. [CrossRef]
112. Gao, X.; Agyakwa, P.A.; Simonelli, M.; East, M.; Hague, R.J.M.; Gilani, N. Tailored Droplet Deposition Strategies for Direct Printing of Fully Functional Components via Molten Metal Jetting. *J. Manuf. Process.* **2025**, *151*, 206–213. [CrossRef]
113. Lass, N.; Gerdes, B.; Jehle, M.; Riegger, L.; Zengerle, R.; Koltay, P. Generation of High Aspect Ratio Metal Microstructures Exhibiting Low Surface Roughness by Drop-Wise Printing of Liquid Metal. *Procedia Eng.* **2015**, *120*, 1103–1106. [CrossRef]
114. Traxel, K.D.; Elton, E.S.; Petersen, A.M.; Silva, C.M.; Perron, A.; Jeffries, J.R.; Pascall, A.J. Processing and Microstructure of a Cu-Al-Fe-Mn Alloy via Droplet-on-Demand Additive Manufacturing. *Mater. Des.* **2024**, *237*, 112544. [CrossRef]
115. Simonelli, M.; Aboulkhair, N.; Rasa, M.; East, M.; Tuck, C.; Wildman, R.; Salomons, O.; Hague, R. Towards Digital Metal Additive Manufacturing via High-Temperature Drop-on-Demand Jetting. *Addit. Manuf.* **2019**, *30*, 100930. [CrossRef]